Journal of Inorganic and General Chemistry
ZAAC
Zeitschrift für anorganische und allgemeine Chemie
www.zaac.wiley-vch.de
RESEARCH ARTICLE

DOI: 10.1002/zaac.202300165

Special Collection

# Alkaline Metal Intercalates of $VSe_2$ by Electrochemical Intercalation

Bastian Kannen[b] and Bertold Rasche*[a, b]

*Dedicated to Prof. Dr. Michael Ruck's 60th Birthday.*

We report on the series of the alkali metal intercalates of $VSe_2$ synthesised by electrochemical means in an aqueous environment. For all alkali metals we find water-conintercalated structures (stage I and stage II), of which only the sodium structure had been reported so far. The new structures are analyzed by powder X-ray diffraction and Rietveld refinement. Their (meta-)stability is investigated in terms of the open circuit potential, revealing the sensitivity towards oxygen. Except for the lithium intercalate these structures transform into water-free alkali metal intercalates under vacuum. In addition, scanning electron microscopy reveals the impact of different electrochemical intercalation techniques yielding different intercalation rates. This paves the way for future single crystal investigations.

## Introduction

Vanadium diselenide $VSe_2$ belongs to the group of layered transition metal dichalcogenides (TMDs), which have recently regained attention as catalysts in the electrochemical hydrogen evolution reaction or as electrode materials in batteries.[1–7] Its structure is of the $CdI_2$ type, in which vanadium centered selenium octahedra form layers via shared edges. As for all layered TMDs, these layers hold together by Van-der-Waals (VdW) interactions, forming an ideal basis for (de-)intercalation of cations and molecules and consequently for electrode materials.[8–10] Indeed, already when $VSe_2$ was first discovered in 1939, Ernst Hoschek and Wilhelm Klemm found evidence for a phase width of the structure and furthermore concluded that this phase width originates from additional vanadium which can "intercalate" into the VdW gap of the $VSe_2$, rendering the phase $V_{1+x}Se_2$.[11] This was later confirmed and further elaborated by Rost et al.[12]

[a] J.-Prof. Dr. B. Rasche
University of Stuttgart
Institute of Inorganic Chemistry
Pfaffenwaldring 55, 70569 Stuttgart
E-mail: bertold.rasche@iac.uni-stuttgart.de
[b] B. Kannen, J.-Prof. Dr. B. Rasche
University of Cologne
Institute for Inorganic Chemistry
Greinstr. 6, 50939 Cologne

Supporting information for this article is available on the WWW under https://doi.org/10.1002/zaac.202300165

*This article is part of a Special Collection dedicated to Professor Michael Ruck on the occasion of his 60th birthday. Please see our homepage for more articles in the collection.*



However, only in 1959 the possibility of a post-synthetic intercalation of this type of material was realized by Rüdorff by intercalating $MoS_2$ and $WS_2$ with the alkaline metals in liquid ammonia.[13–15] This concept expanded quickly, regarding the used TMDs, as well as the used methods.[16–18] Initially, further chemical methods, e.g. the intercalation with n-buthyllithium were reported, which is also the first chemical method which was employed to intercalate $VSe_2$.[19,20] Subsequently, in 1974 several groups reported the first electrochemical intercalation of TMDs.[21–23] While some of the first electrochemical TMD experiments were based on aqueous solutions,[21,23] this quickly shifted toward aprotic organic solvents such as oxolane or propylene carbonate.[21,22,24] For that reason, in 1978 the first electrochemical intercalation of $VSe_2$ was in oxolane and already with the idea of an electrode material in mind.[25] Consequently, up to date only one intercalate of $VSe_2$ with co-intercalated water has been structurally characterized,[26] while several water-free alkali metal intercalates $A_xVSe_2$ with $x$ ranging from 0.2 up to 2 are known.[19,20,27–31] All these intercalated $VSe_2$-structures were synthesized chemically.

In addition, the authors reported on one selected intercalate, lacking the basis to investigate overall trends within e.g. the series of alkali metal intercalates. While this can be beneficial when it comes to applications as electrode materials in batteries, the latter is particularly of interest, as many of the TMDs exhibit unusual physical properties such as superconductivity. These superconducting properties could be changed substantially by intercalation with different types of ions and molecules, providing an ideal playground for insights into the superconducting state.[17,32,33,2,34,35]

This work is the first comprehensive report on the electrochemical intercalation of $VSe_2$ with the whole series of the alkaline metals in an aqueous environment. The new structures are analyzed by powder X-ray diffraction. Their (meta-)stability is investigated in terms of the open circuit potential, revealing the sensitivity towards oxygen. For the heavier alkali metal intercalates we demonstrate that water can be removed via

 

vacuum to form the water-free structure. In addition, scanning electron microscopy reveals the impact of different electrochemical intercalation techniques employing different intercalation rates.

## Results and Discussion

### *Synthesis*

Phase pure $VSe_2$ (1T-polytype; Pearson symbol: *hP3*) powder and crystals with dimensions up to 100×100×5 $\mu m^3$ were synthesized from the elements in a V:Se ratio of 1:2 at 720 °C in sealed quartz ampoules (Supporting Information – SI: Figure S1; details see experimental section). For the intercalation reactions, $VSe_2$ has to be synthesized in this precise ratio, because excess vanadium is known to occupy the VdW gap.[10,36] Larger $VSe_2$ single crystals with average dimensions of 500×500×20 $\mu m^3$ were grown by chemical vapor transport in a 820 °C to 870 °C gradient.

The powder was immersed in a carbon composite and dropcasted onto glassy carbon electrodes ($VSe_2$-GCE) or onto carbon fibers ($VSe_2$-CF), which were then used as working electrodes in the electrochemical experiments. With a similar carbon composite the single crystals were attached to the end of a carbon sticks and also used as working electrodes ($VSe_2$-SC-CS).

### *Electrochemical Intercalation of $VSe_2$ with Alkali Metals*

A $VSe_2$-GCE was immersed in aqueous 0.1 M solutions of either LiCl, NaCl, KCl, RbCl or CsCl. In a cyclo voltammetric (CV) experiment the potential was swept from the equilibrium state (open circuit potential – OCP) to −1.5 V (all listed potentials are referenced to an Ag/AgCl 3 M NaCl reference) and reversed to 0.05 V with a scan rate of 2 $mVs^{-1}$ in 2 cycles (Figure 1). The CV was paused at the most negative potential (−1.5 V) and the OCPs of the reduced species were measured for 30 minutes (SI: Figure S3). CVs without pausing were also recorded (SI: Figure S2).

The CVs with the electrolytes containing LiCl, NaCl, KCl, RbCl and CsCl show one cathodic peak (peak **C1**) in the reductive scans at about −1.05 V, −0.98 V, −1.00 V, −1.02 V and −0.93 V, respectively. In the potential range of these peaks the hydrogen evolution reaction slowly starts and yields an increasing background current, although the respective current only strongly increases for potentials more negative than −1.3 V. For the second cycles, another group of small reductive peaks appear (peaks **C2**) at about −0.70 V, regardless of the alkali metal cation.

The oxidative scan has one peak (peak **A1**) for the LiCl, NaCl, KCl, RbCl and CsCl solutions at −0.54 V, −0. 39 V, −0.42 V, −0.34 V and −0.32 V, respectively. A second small peak (peak **A2**) is starting to show at −0.15 V, regardless of the alkali metal cation.

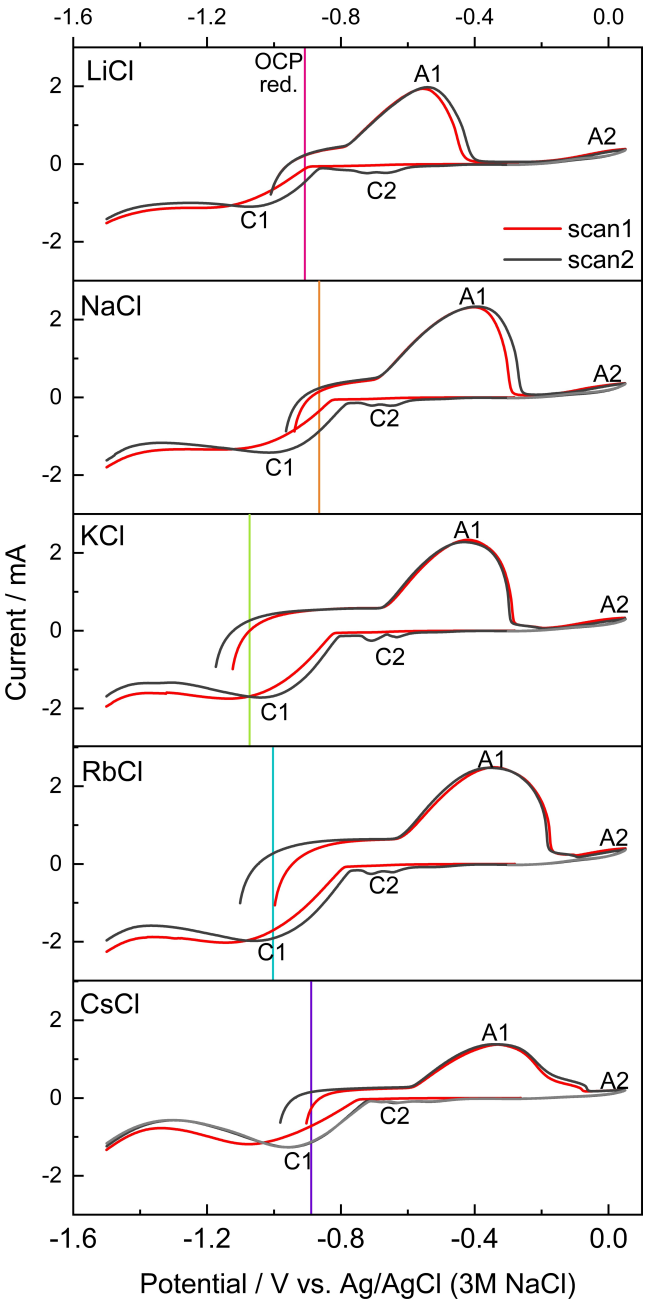


**Figure 1.** Cyclic voltammograms of $VSe_2$-GCE immersed in 0.1 M *A*Cl (*A* = Li, Na, K, Rb, Cs) solution for 2 cycles with the potential swept from the OCP to −1.5 V vs Ag/AgCl (3 M NaCl) and back to 0.05 V after pausing and measuring the OCPs of the reduced species. The OCPs are indicated after 30 min as vertical lines. Complete OCPs are shown in SI: Figure S3.

We assign reversible processes to the dominant signals **C1**/**A1** and suggest this process to be the intercalation/deintercalation of the alkali metal ions *A* into $VSe_2$, according to Equation (1):

$$VSe_2 + xA^+ + yH_2O + xe^- \rightleftharpoons A_x(H_2O)_yVSe_2. \quad (1)$$

The intercalation of the ion $A^+$ ($A$ = Li, Na, K, Rb, Cs) is accompanied by the co-intercalation of water as will be discussed below. The slight shift of the intercalation signal **C1** most likely results from the higher intercalation barrier for the alkali metal ions at the $VSe_2$ grains in the first cycle,[37] as in subsequent cycles the signal does not shift any further (SI: Figure S6). Because the OCP stabilizes in all cases at a potential below the deintercalation signal (Figure 1 and Figure S3), the formed intercalates can be considered metastable and do not decompose. The variation between the alkali metals are non-systematic and follow from small differences at the electrode surface. Therefore, the OCPs can be considered equal within the error bar.

The small signal **A2** is assigned to the oxidative decomposition of $VSe_2$ for example according to Equation (2):

$$VSe_2 \rightarrow Se + V^{2+} + 2e^- \quad (2)$$

(Further possible decomposition mechanisms can be derived from the Pourbaix diagrams SI: Figure S5). Subsequently, **C2** most likely represents the reduction of the decomposition products, particularly the selenium, according to Equation (3):

$$Se + 2e^- + H_2O \rightarrow HSe^- + OH^- \quad (3)$$

The formed $HSe^-$ can dissolve not yet reduced selenium forming polyselenides,[38] which is indeed what we observe (SI: Figure S4). Consequently, by lowering the upper potential limit of the CV experiment to −0.2 V, the peaks **A2** and **C2** can be eliminated (SI: Figure S2). The latter potential range was used for all further experiments.

### *Structure Analysis of Alkali Metal Intercalated $VSe_2$*

The electrochemical proposed intercalation is confirmed by ex situ powder X-ray diffraction (PXRD). The intercalated compounds $A_x(H_2O)_yVSe_2$ were prepared by CV experiments of $VSe_2$-CF electrodes in 0.1 M alkali metal chloride solutions. After cycling the potential between −0.2 V and −1.5 V with 2 $mVs^{-1}$ once, the experiment was stopped at the reductive potential of −1.5 V and the (now reduced) $VSe_2$-CF electrodes were taken from the solution and sealed in glass capillaries. This allowed subsequent characterization by PXRD. In a second set of experiments, analogically reduced $VSe_2$-CF electrodes were evacuated over night after removal from the solution and before sealing them in glass capillaries and measuring PXRD.

The non-evacuated reduction products all have similar diffraction patterns, except for the experiment with sodium. In all cases, the patterns are distinctly different from the original $VSe_2$ pattern (Figure 2a). The dramatic shift of the first diffraction peak (001) toward smaller $2\theta$ angles already indicates an intercalation, as this peak directly relates to the interlayer distance, which increases. Rietveld refinement (SI: Figure S7 and Table S1 to S4) allows to further evaluate the structures. Except for sodium, all alkali intercalates are similar with a single layer of alkali metal atoms (and water molecules, see below) within the van der Waals gap between the $VSe_2$ layers in a trigonal prismatic coordination of selenium atoms and statistical occupancy (so-called stage I structure). Besides the increased distance between the $VSe_2$ layers due to the intercalation, this also results in a shift of the $VSe_2$ layers, yielding a 3R-type structure (Figure 2c). The structure found in case of the sodium intercalate matches with the so-called stage II co-intercalate of sodium and water in which sodium within the VdW gap is octahedrally surrounded by six water molecules (SI: Figure S8).[25,26] This leads to an even further increase in the $VSe_2$ interlayer distance immediately recognizable in the diffraction pattern. However, a small diffraction peak at approximately 4.5° $2\theta$ indicates that most likely also the structure type of the other alkali metal intercalates, the stage I intercalate, is partially or as intermediate formed with sodium.

The stage II intercalate in case of sodium is already a strong indication of the co-intercalation of water. Moreover, for the other alkali metals the same interlayer spacing is observed independently of the intercalated alkali ion and on evacuation we observe substantial structural changes (Figure 2). We conclude that all alkali metals are co-intercalated with water, thus being the stage I co-intercalate of the alkali metals and water.[25,26] Consequently, we assign a mixed occupation of the alkali metal sites with oxygen from water. It shall be mentioned, that due to the intercalation process being performed in a CV experiment with high intercalation rates, the crystallites are most likely heavily strained and probably affected by stacking faults, making the Rietveld fit challenging (see discussion in the SI: Table S1).

As the intercalation is performed electrochemically, the alkali metal content $x$ in $A_x(H_2O)_yVSe_2$ can be calculated by applying Faraday's law to the charge $q$ from the integrated deintercalation peaks **A1** (SI: Figure S9) by the following Equation (4):

$$n(A^+) = \frac{q}{z \cdot F} = \frac{\int I \mathrm{d}\Phi}{z \cdot F \cdot 2\frac{mV}{s}}; \quad x = \frac{n(A^+)}{n(VSe_2)} \quad (4)$$

where $n$ is the amount of substance, $I$ the current, $\Phi$ the potential, $z$ the charge of the intercalated ion (here $z = 1$) and F the Faraday constant. All alkali metal intercalates form structures with $x \approx 0.2$–$0.3$, which further strengthens the model developed by Rietveld refinement. The alkali metal content also coincides with water-free synthesis of Na, K and Cs intercalates of $VSe_2$ by Brauer et al.[31]

Upon evacuation of the obtained intercalates, yet different diffraction patterns are observed (Figure 2b), suggesting removal of co-intercalated water, as mentioned above. Particularly, the (001) diffraction peak is now shifted towards slightly higher $2\theta$ angles and varies between the different alkali cations, indicating smaller interlayer distances between the $VSe_2$ layers, which now correlate with the expected ionic radii (Figure 2d). The diffraction pattern of the evacuated $Li^+$ intercalated structure differs from those with $Na^+$, $K^+$, $Rb^+$ and $Cs^+$. The pattern shows broad peaks and resembles the pattern of $VSe_2$, indicating the decomposition of the $Li_x(H_2O)_yVSe_2$ structure:

 

Journal of Inorganic and General Chemistry
ZAAC
Zeitschrift für anorganische und allgemeine Chemie



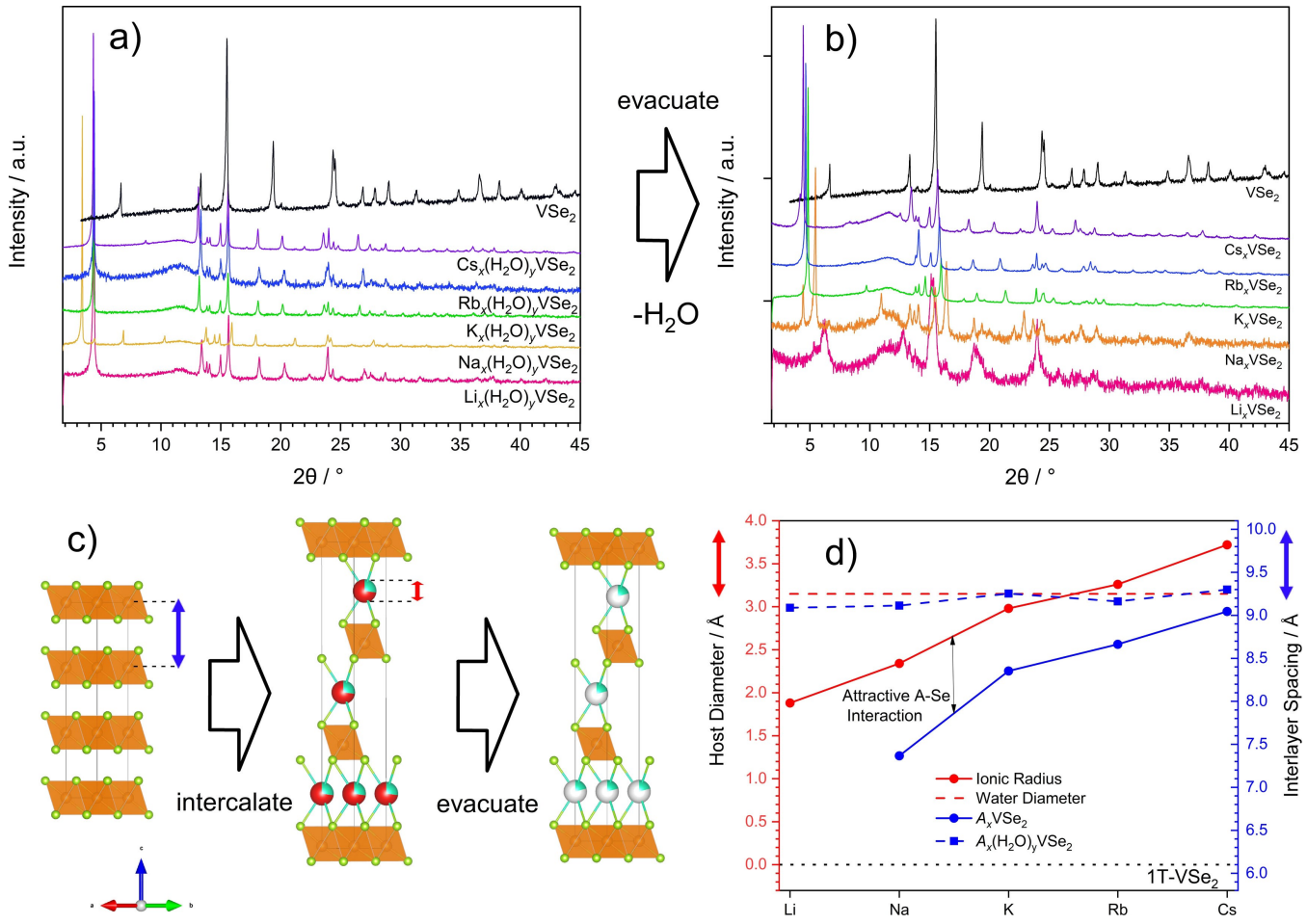


**Figure 2.** Powder X-Ray diffractograms of a) $VSe_2$ reduced in 0.1 M *A*Cl (*A* = Li, Na, K, Rb, Cs) solution and b) analogous prepared compounds after evacuating over night (All underlying CVs are shown in the SI: Figure S6). c) shows exemplary structures of 1T-VSe2 (left), Cs and water co-intercalated $VSe_2$ (middle) and Cs intercalated $VSe_2$ without co-intercalated water (right) with V (orange), Se (green), Cs (blue) and Oxygen (red). All structure parameters are listed in the SI Table S1 to S4. d) summarizes the relation between host diameter and the *c*-axis.

$$Li_x(H_2O)_yVSe_2 \rightarrow xLiOH + \frac{x}{2}H_2 + VSe_2 + (y - x)H_2O. \quad (5)$$

The broad peaks would follow from a low crystallinity of the $VSe_2$. We speculate, that the small ionic radius of the $Li^+$ cation is responsible for the instability of this water-free type of structure. The other water-free intercalates form structures similar to their non-evacuated relatives (SI: Figure S7), although for sodium the removal of water might not be complete. We speculate that this is due to the water-rich stage II intercalate.

A summary of the change in the interlayer distance upon intercalation and evaporation of all intercalated structures is shown in Figure 2d (For sodium we used the *c*-value from the stage I intercalate). The left axis represents the diameter of the intercalated host and the right axis the resulting interlayer distance. The interlayer distance of all intercalated structures is larger than the one present in $VSe_2$ (6.10 Å). As mentioned above, the *c*-axis of the compounds $A_x(H_2O)_yVSe_2$ is constant within the error limits indicating a co-intercalation of water. In such a co-intercalated structure, the interlayer distance is defined by the diameter of the water molecule (up to 3.4 Å depending on the orientation[39]), as this diameter of water is larger (or similar for the $Cs^+$) to the diameters of the alkali metal ions (1.88 to 3.72 Å[40]). Furthermore, the elongation along the c-axis of 3.0–3.2 Å matches well with the diameter of the water molecule of 3.4 Å. Upon evaporation, the interlayer distance gets smaller and, most importantly, now depends on the ionic radii of the unhydrated cations.[40] However, the measured interlayer space is about 1 Å smaller than the spacing expected by purely steric elongation. We attribute this effect to the attractive Coulomb interactions between the negatively charged $VSe_2$-layers and the cations, replacing the VdW interactions in $VSe_2$. The V–Se distances for all intercalated structures range from 2.46 to 2.52 Å (SI: Table S5), which coincides with interatomic distances of intercalated $VSe_2$ known from the literature (2.35 to 2.61 Å) and with the 2.50 Å in the non-intercalated structure.[26,27,29,41,42]

 

### *Stability of Alkali Metal Intercalated $VSe_2$*

To examine the air stability of the intercalated species, $VSe_2$-CF electrodes were intercalated via linear sweep voltammetry (LSV) outside of the glovebox, while still working in a degassed 0.1 M aqueous solutions of LiCl, NaCl, KCl, RbCl and CsCl and under a dynamic argon atmosphere. The latter setup still allows for small traces of oxygen to diffuse into the solution. These slightly increased oxygen concentrations are ideal to test the sensitivity of the material. Under these conditions, the OCPs of the intercalated compounds were measured over a duration of 50 minutes.

In contrast to the OCPs measured inside the glove box, all OCPs measured outside exhibit a distinct step in the potential curve after varying times (Figure 3a), namely at 5, 20, 28, 32, and 35 minutes for the $Na^+$, $Cs^+$, $K^+$, $Rb^+$ and $Li^+$ intercalates, respectively. These steps indicate the decomposition of the $A_x(H_2O)_yVSe_2$ ($A$ = Li, Na, K, Rb, Cs) compounds, with the OCP reaching the equilibrium value corresponding to the non-intercalated $VSe_2$ structure. We therefore assign the oxidation of the intercalated compounds by oxygen:

$$A_x(H_2O)_yVSe_2 + \frac{x}{4}O_2 + \frac{x}{2}H_2O \rightarrow VSe_2 + yH_2O + xAOH. \quad (6)$$

This demonstrates the sensitivity of the metastable compounds towards air, which makes working under argon imperative.

Additionally, independent of whether the OCP was measured inside or outside the glove box, the curves always slightly differ in their shape and the sequence of the final potentials with regard to the used alkali metal. Most likely, this can be attributed to small traces of decomposition products or other impurities at the electrode and represents the error of the OCP. However, in all cases the potential initially stabilizes at a more negative potential than that of the deintercalation peak (compounds are metastable). Only in the presence of oxygen we observe the distinct jump to a potential above that of the deintercalation peak, which indicates the decomposition of the compound in the presence of oxygen traces.

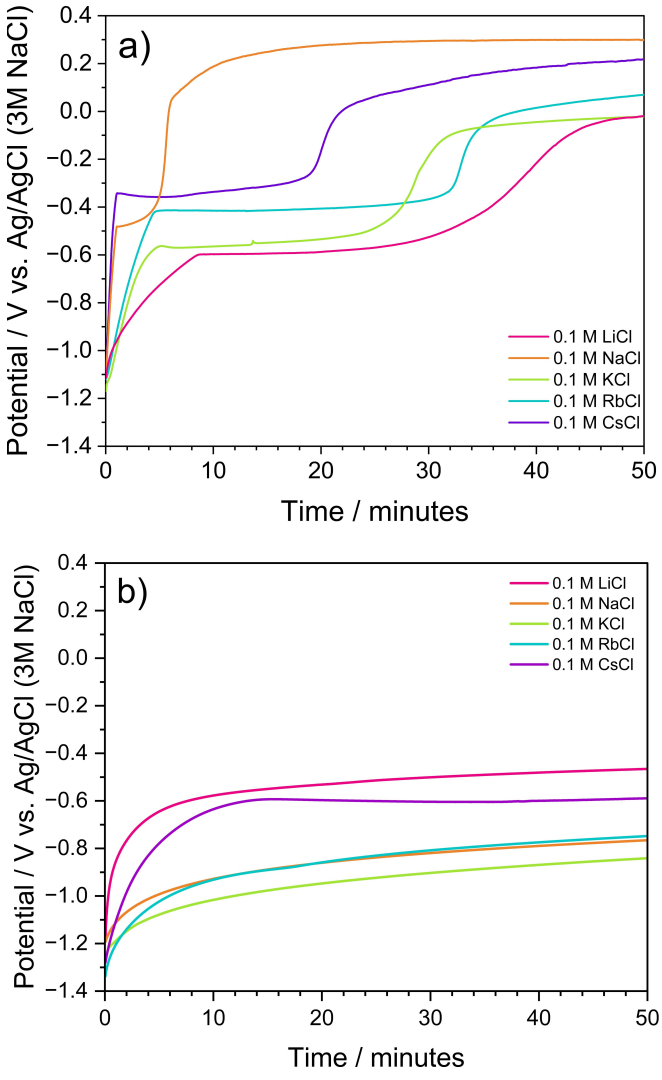


**Figure 3.** Open circuit potentials of a) $VSe_2$-CF electrodes or b) $VSe_2$-SC-CS elecctrodes immersed in 0.1 M *A*Cl ($A$ = Li, Na, K, Rb, Cs) solution after linear sweep voltametric experiments with a potential swept from the OCP to −1.5 V vs Ag/AgCl (3 M NaCl) while a) outside the glovebox at a dynamic argon atmosphere or b) in an argon glovebox.

### *Influence of Crystal Size and Intercalation Rate*

To understand the impact of different intercalation rates, which is of major importance for future single crystal experiments, electrochemical experiments were conducted with $VSe_2$ single crystals and their morphology was analyzed via scanning electron microscopy (SEM). CV experiments as described above were compared to chronopotentiometry (CP) experiments. For electrochemical intercalation reactions, the intercalation rate is directly proportional to the current, because each electron corresponds to one intercalated ion. For CV experiments the current changes during the experiment and is relatively high, as it peaks once the potential reaches the necessary value for the intercalation and is only limited by mass transport, probably inside the crystal. In contrast, for the CP experiment, a constant current is employed guaranteeing a constant (slow) intercalation rate. Within this context, also the influence of the crystal size was examined.

Crystals of different dimensions (see synthesis section) were attached to a carbon fiber stick and immersed in aqueous CsCl solution. Smaller crystals with dimensions 100×100×100 $\mu m^3$ were held at a reductive current of −200 nA for 30 minutes. Larger Crystals synthesized with dimensions 500×500×20 $\mu m^3$ were held at −400 nA for about an hour and at −800 nA for another hour.

The CPs (Figure 4) show an intercalation with a current of −200 nA at a constant potential of −0.81 V for smaller crystals. The completion of the intercalation is indicated by a potential drop, where the newly reached potential corresponds to the hydrogen evolution reaction (HER) judging from slowly forming

 

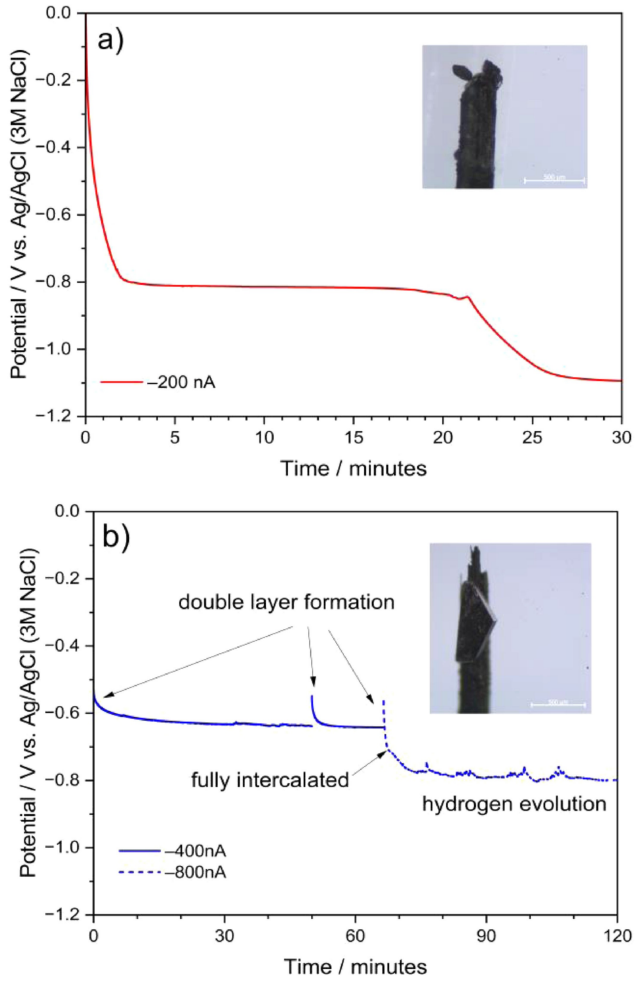


**Figure 4.** Chronopotentiometry experiments with $VSe_2$ single crystals with dimensions of about a) 100×100×5 μm³ and b) 500×500×20 μm³ on carbon fiber sticks immersed in 0.1 M CsCl solution. For b) the current was briefly paused two times after about 50 and 60 minutes, resulting in non-faradaic currents at higher potentials.

bubbles. Larger crystals were intercalated with a larger current of −400 nA to achieve comparable current densities. The intercalation is still ongoing after 65 minutes at −0.63 V. After few minutes at −800 nA, the end of the intercalation is once again indicated by a drop to the potential of the HER. Due to the higher absolute current the potential curve exhibits spikes because of the fast formation of $H_2$-bubbles. It shall be noted that many of the intercalation attempts with larger transport crystals showed uneven and unreproducible current flows, which might be due to contacting problems (SI: Figure S10–11). These problems were not encountered with the smaller crystals, which were hence used to study the morphology of the crystals at different intercalation rates by SEM.

Exemplarily, $VSe_2$-SC-CS electrodes were immersed in a 0.1 M CsCl solution and intercalated in a LSV experiment at 1 $mVs^{-1}$ with a peak current of ≈−3000 nA (OCP to −1.5 V) or a CP experiment at constant −200 nA (Figure 5d/g).

For all crystals, whether before the intercalation or after the LSV or the CP intercalation, the layered structure is apparent in the the SEM images (Figure 5). However, in contrast to the non-intercalated $VSe_2$, all intercalated crystals show also a splitting of layers. We assign this to the decoupling of layers during the intercalation of the alkali metal ions into the $VSe_2$ host. However, this could also follow from a chemical deintercalation according to equation (6), as the crystals were briefly exposed to air before SEM imaging. We therefore focus on the comparison on the two types of intercalations. Crystals intercalated by LSV (peak current ≈−3000 nA) have a wavy, uneven surface in contrast to those intercalated constantly with −200 nA. Most likely this follows from a fast and more chaotic intercalation process caused by an approximately 15x higher intercalation rate. Most likely, the slow diffusion of the ions inside the crystals leads to a "blow up" of the layers at the edge of the crystal, while the inner region of the crystal is not yet intercalated. Crystals were also intercalated at constant potentials with an even higher intercalation rate (SI: Figure S13). However, these crystals were not characterized by SEM, as the crystals detached from the electrode due to the high currents.

## Conclusions

The alkali metal intercalates $A_x(H_2O)_yVSe_2$ ($A$ = Li, Na, K, Rb, Cs) ($0.2 < x < 0.3$) were synthesized by electrochemical means in an aqueous system. According to Rietveld refinements, all of these alkali metal intercalates crystalize in the same structure known as stage I intercalate, with the exception of sodium which forms the so-called stage II intercalate. In the stage I intercalate the alkali metal atoms and water statistically occupy the trigonal prismatic voids in the $VSe_2$ VdW gaps. Under vacuum, the co-intercalated water can be removed, yielding new crystal structures $A_xVSe_2$ for $A$ = Na, K, Rb, Cs. $Li_xVSe_2$ however cannot be obtained under these conditions as it decomposes to $VSe_2$. All intercalated vanadium diselenides are air sensitive and deintercalate within few minutes even at low oxygen partial pressures. The influence of the intercalation rate could be demonstrated by intercalation of single crystals and their characterization by SEM imaging.

## Experimental Section

### *Synthesis*

1T-$VSe_2$ powder was synthesized from the elements in an oven synthesis. Vanadium and selenium (1:2) were sealed in a quartz ampoule under inert conditions. The ampoule was heated to 720 °C (2 K/min), held for 4 days and cooled to room temperature. The yielded $VSe_2$ powder contained single crystals with dimensions of 100×100×5 μm³ which were isolated. PXRD measurements indicate phase pure $VSe_2$. Larger crystals with the dimensions 500×500×20 μm³ were synthesized from the elements in sealed quartz ampoules in a chemical vapor transport reaction ($T_1$ = 820 °C, $T_2$ = 870 °C) with Iodine as transport agent (0.5 mg/cm³).[43]

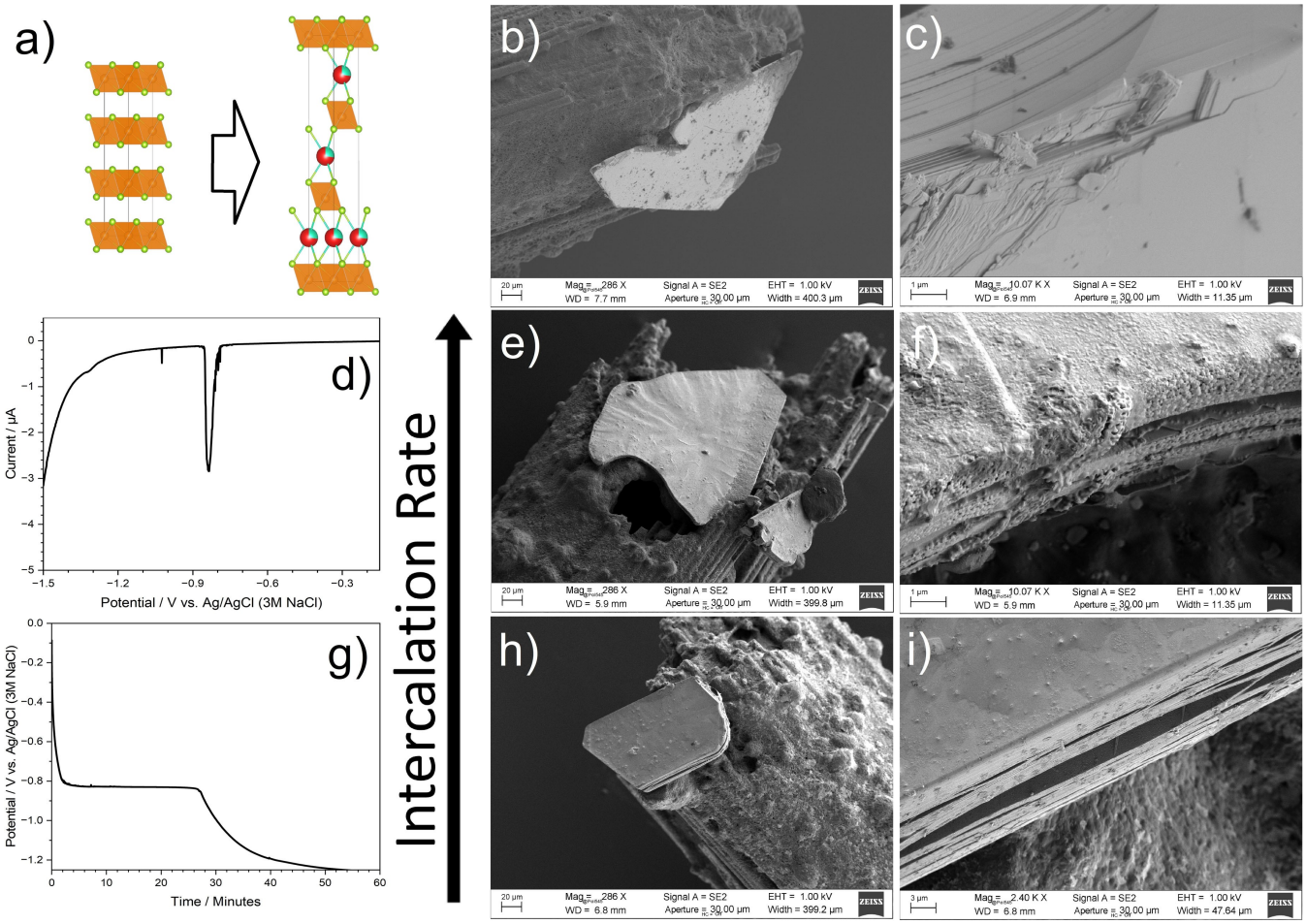


**Figure 5.** a) Structures of 1T-$VSe_2$ and $Cs_x(H_2O)_yVSe_2$ with V (orange), Se (green), Cs (blue) and O (red). Graphs of a d) linear sweep voltammetry (1 $mVs^{-1}$) and g) chronopotentiometry (−200 nA) experiment with $VSe_2$-SC-CS electrodes immersed in 0.1 M CsCl solution. Corresponding SEM images of b)/c) the unintercalated $VSe_2$ and Cs intercalated $VSe_2$ by e)/f) linear sweep voltammetry and h)/i) chronopotentiometry. Additional SEM images are shown in the SI (Figure S12).

Lithium chloride, sodium chloride, potassium chloride, rubidium chloride and cesium chloride were purchased from Sigma-Aldrich and used without further purification. 0.1 M solutions were prepared with deionized water (0.055 µS/cm) and degassed with argon (also in the glove box).

### *Electrochemical Experiments*

All experiments were performed at room temperature. All experiments except those exploring air stability, were performed in an argon filled glovebox. Experiments outside the glovebox were performed in a dynamic argon atmosphere after stormy degassing the electrolytes for 10 min. A three electrode setup, consisting of a graphite counter electrode, a Ag/AgCl (3 M NaCl) (inside the glovebox) or a leakless Ag/AgCl (outside the glovebox) reference electrode and the working electrodes described below was used. For experiments with the $VSe_2$ powder, a composite was prepared from $VSe_2$, carbon black and polyvinylidene fluoride with an approximate weight ratio of 85:10:5 in N-methylpyrrolidone. After proper stirring, the composite was applied to either a freshly polished glassy carbon electrode (GCE) or to the end of a twisted bunch of carbon fibers (CF, 7 µm ∅, R&G GmbH). Crystals were applied to carbon fiber sticks (CS, 0.28 mm ∅, R&G GmbH) with a composite of carbon black and polyvinylidene fluoride (PVDF) in dimethylformamide.

### *Powder X-Ray Diffraction*

Powder X-Ray Diffraction (PXRD) of 1T-$VSe_2$ was performed with Cu-$K_\alpha$ radiation with a Rigaku MiniFlex diffractometer (Ni-foil filter, D/teX Ultra detector) in Bragg-Brentano geometry. $VSe_2$ was intercalated on CF electrodes. The intercalated compounds were sealed in 0.9 mm capillaries along with the CF electrodes and characterized with Mo-$K_\alpha$ radiation on a STOE Stadi P diffractometer (Ge-monochromator, Mythen 1 K detector) in Debye-Scherrer geometry.

### *Rietveld*

Rietveld refinement was performed with TOPAS Academic Version 6.[44] The peak shape was described by a fundamental parameter approach and a set of parameters (Lorentz and Gaussian functions) for each phase to account for strain, etc. related broadening. The background was described by 7 Chubychev polynomials. An additional peak at 11.5° $2\theta$ was added to account for the diffraction from the amorphous carbon contents of the electrode. Occupancies

 

$y_{PXRD}$ and $x_{PXRD}$ are refined with restriction for the water co-intercalate and the water-free intercalate, respectively. Deviations of the occupancies from the values expected from the electrochemical experiments indicate the possible issue of a shared vanadium/alkali metal occupancy, something known from the alkali metal intercalates of FeSe.[45] This is not further evaluated as the data is not sufficient to draw final conclusions.

### *Scanning Electron Microscopy*

The morphology of $VSe_2$ and $Cs_x(H_2O)_yVSe_2$ single crystals was characterized by scanning electron microscopy (SEM) with a Zeiss Sigma 300 VP at an approximate working distance of 6 mm at an acceleration voltage of 1 kV employing the secondary electron (SE) detector.

All figures were prepared with VESTA[46] and OriginLab2022.[47]

## Acknowledgements

We would like to thank Sebastian Bette and Simon Cassidy for their support with the Rietveld refinements. We thank Ziyaad Aytuna for support taking the SEM images. B.R. acknowledges funding via a Liebig-Group by the FCI. Open Access funding enabled and organized by Projekt DEAL.

## Conflict of Interest

The authors declare no conflict of interest.

## Data Availability Statement

The data that support the findings of this study are available from the corresponding author upon reasonable request.

**Keywords:** electrochemical intercalation · transition metal chalcogenides · vanadium selenide · alkaline metal intercalates · intercalation rate

[1] Y. Wang, B. Qian, H. Li, L. Liu, L. Chen, H. Jiang, *Mater. Lett.* **2015**, *141*, 35–38.
[2] Z. Wang, R. Li, C. Su, K. P. Loh, *SmartMat* **2020**, e1013, DOI 10.1002/smm2.1013.
[3] G. G. Naumis, in *Synthesis, Modeling, and Characterization of 2D Materials, and Their Heterostructures*, Elsevier, **2020**, pp. 77–109.
[4] B. Chen, D. Chao, E. Liu, M. Jaroniec, N. Zhao, S.-Z. Qiao, *Energy Environ. Sci.* **2020**, *13*, 1096–1131.
[5] W. Wang, L. Ran, R. Hu, C. Zhang, R. Huang, Y. Li, Y. Ouyang, J. Yan, *SSRN Journal* **2022**, DOI 10.2139/ssrn.4211511.
[6] X. Wang, H. Zhou, Z. Chen, X. Meng, *Energy Storage Mater.* **2022**, *49*, 181–208.
[7] D. Sha, Y. You, R. Hu, X. Cao, Y. Wei, H. Zhang, L. Pan, Z. Sun, *Adv. Mater.* **2023**, *35*, 2211311.
[8] M. Salavati, T. Rabczuk, *Comput. Mater. Sci.* **2019**, *160*, 360–367.
[9] J. F. Smith, *Phase Diagrams of Binary Vanadium Alloys*, ASM International, Metals Park, Ohio, **1989**, 256–261.
[10] K. Kang, S. Chen, E.-H. Yang, in *Synthesis, Modeling, and Characterization of 2D Materials, and Their Heterostructures*, Elsevier, **2020**, pp. 247–264.
[11] E. Hoschek, W. Klemm, *Z. Anorg. Allg. Chem.* **1939**, *242*, 49–62.
[12] E. Røst, L. Gjertsen, *Z. Anorg. Allg. Chem.* **1964**, *328*, 299–308.
[13] W. Rüdorff, H. H. Sick, *Angew. Chem.* **1959**, *71*, 127–127.
[14] W. Rüdorff, *Angew. Chem.* **1959**, *71*, 487–491.
[15] W. Rüdorff, *Angew. Chem.* **1966**, *78*, 948–948.
[16] A. D. Yoffe, *Annu. Rev. Mater. Sci.* **1973**, *3*, 147–170.
[17] F. R. Gamble, T. H. Geballe, in *Treatise on Solid State Chemistry: Volume 3 Crystalline and Noncrystalline Solids* (Ed.: N. B. Hannay), Springer US, Boston, MA, **1976**, pp. 89–166.
[18] R. Schöllhorn, *Physica B + C* **1980**, *99*, 89–99.
[19] M. B. Dines, *Mater. Res. Bull.* **1975**, *10*, 287–291.
[20] D. W. Murphy, F. J. Di Salvo, G. W. Hull, J. V. Waszczak, *Inorg. Chem.* **1976**, *15*, 17–21.
[21] M. S. Whittingham, *J. Chem. Soc., Chem. Commun.* **1974**, *9*, 328–329.
[22] G. V. S. Rao, J. C. Tsang, *Mater. Res. Bull.* **1974**, *9*, 921–926.
[23] R. Schöllhorn, H. Meyer, *Mater. Res. Bull.* **1974**, *9*, 1237–1245.
[24] D. A. Winn, J. M. Shemilt, B. C. H. Steele, *Mater. Res. Bull.* **1976**, *11*, 559–566.
[25] M. S. Whittingham, *Mater. Res. Bull.* **1978**, *13*, 959–965.
[26] A. J. A. Bos-Alberink, R. J. Haange, G. A. Wiegers, *J. Less-Common Met.* **1979**, *63*, 69.
[27] J. R. Bloembergen, R. J. Haange, G. A. Wiegers, *Mater. Res. Bull.* **1977**, *12*, 1103–1110.
[28] C. F. Van Bruggen, J. R. Bloembergen, A. J. A. Bos-Alberink, G. A. Wiegers, *Journal of the Less Common Metals* **1978**, *60*, 259–282.
[29] Y. Watanabe, G. A. Wiegers, C. F. Van Bruggen, *Synth. Met.* **1984**, *10*, 1–4.
[30] H. E. Brauer, H. I. Starnberg, L. J. Holleboom, H. P. Hughes, *Surf. Sci.* **1995**, *331–333*, 419–424.
[31] H. E. Brauer, H. I. Starnberg, L. J. Holleboom, V. N. Strocov, H. P. Hughes, *Phys. Rev. B* **1998**, *58*, 10031–10045.
[32] G. A. Wiegers, *Physica B + C* **1980**, *99*, 151–165.
[33] R. H. Friend, A. D. Yoffe, *Adv. Phys.* **1987**, *36*, 1–94.
[34] B. Rasche, M. Yang, L. Nikonow, J. F. K. Cooper, C. A. Murray, S. J. Day, K. Kleiner, S. J. Clarke, R. G. Compton, *Angew. Chem. Int. Ed.* **2019**, *58*, 15401–15406.
[35] B. Rasche, *Curr. Opin. Electrochem.* **2021**, *25*, 100630.
[36] E. Røst, L. Gjertsen, *Z. Anorg. Allg. Chem.* **1964**, *328*, 299–308.
[37] R. Schöllhorn, *Angew. Chem. Int. Ed. Engl.* **1980**, *19*, 983–1003.
[38] B. Rasche, H. M. A. Amin, S. J. Clarke, R. G. Compton, *J. Electroanal. Chem.* **2019**, *835*, 239–247.
[39] J. L. Finney, *J. Mol. Liq.* **2001**, *90*, 303–312.
[40] A. G. Volkov, S. Paula, D. W. Deamer, *Bioelectrochem. Bioenerg.* **1997**, *42*, 153–160.
[41] B. Deng, F. Q. Huang, D. E. Ellis, J. A. Ibers, *J. Solid State Chem.* **2005**, *178*, 3251–3255.
[42] K. Hayashi, M. Nakahira, *J. Solid State Chem.* **1978**, *24*, 153–161.
[43] M. Binnewies, Ed., *Chemische Transportreaktionen*, De Gruyter, Berlin; New York, **2011**, 391.
[44] A. A. Coelho, *J. Appl. Crystallogr.* **2018**, *51*, 210–218.
[45] N. R. Davies, M. C. Rahn, H. C. Walker, R. A. Ewings, D. N. Woodruff, S. J. Clarke, A. T. Boothroyd, *Phys. Rev. B* **2016**, *94*, 144503.
[46] K. Momma, F. Izumi, *J. Appl. Crystallogr.* **2011**, *44*, 1272–1276.
[47] Origin2022, OriginLab, Northhampton, **2023**, https://www.originlab.com/.

Manuscript received: July 25, 2023
Revised manuscript received: November 10, 2023
Accepted manuscript online: November 29, 2023

 